Hydrodynamic signatures and spectral properties of the quantum vortex

João E. H. Braz [1], P. Ribeiro [1], and H. Terças [2]
[1] *CeFEMA, Instituto Superior Técnico, Universidade de Lisboa, 1049-001 Lisboa, Portugal*
[2] *IPFN, Instituto Superior Técnico, Universidade de Lisboa, 1049-001 Lisboa, Portugal*

(Received 9 March 2022; revised 23 August 2022; accepted 11 October 2022; published 7 November 2022)

We characterize the low-lying excitations of a quantum vortex in a quasi-two-dimensional Bose-Einstein condensate (BEC) using the standard definition of the density of states (DOS) and a modified version that is sensitive to complementary aspects of the excitation's spectrum. The latter proves to be particularly relevant to studying the polaronic state realized when an impurity is embedded in a quantum vortex. We establish that the impurity becomes sensitive to the transversal fluctuations of the vortex, via its remnant kelvon mode, and to the phase fluctuations of the BEC Nambu-Goldstone mode. The presence of the vortex yields an anomalous excitation spectrum with a finite energy gap and nonlinear DOS at low energies. We find that the high sensitivity of the kelvon mode to external potentials provides a quantum-level control channel over impurities trapped in a vortex. This extra control channel may be of practical use for the proposal of using vortex-trapped impurities as qubit units for quantum information processing.

DOI: 10.1103/PhysRevA.106.053305

I. INTRODUCTION

Bose-Einstein condensates (BECs) host a variety of topological defects emerging collectively from the interactions among their constituent atoms. Notable examples are vortex configurations occurring in three-dimensional and in quasi-two-dimensional (quasi-2D) BECs. Their vorticity is quantized and the singularity in the phase of the BEC's order parameter causes the fluid to deplete with a long-range density profile [1]. Although a single-charge vortex is dynamically stable and topologically protected from dissipation [2], the system features multiple dynamics. For one, the vortex is intrinsically subject to the transversal excitations of its filament, known as kelvon modes; these can precipitate the vortex off its rotational axis, triggering an outwards precessional motion that eventually drives it to the boundary [3–11]. Once the vortex is removed then so is the phase singularity, and the BEC is left to evolve according to its intrinsic dynamics alone: the fluid undergoes quantum diffusion [12], driven by the Nambu-Goldstone (NG) mode inherent to the BEC state. One of our main results is to show how these two modes—a kelvon and the NG mode—have also an exceptional capacity to drive the dynamics of impurities embedded in the quantum fluid.

The physics of a BEC in the presence of impurities (e.g., heterogeneous atomic species) has aroused interest in both theory and experiment over the past decade [13–20]; of particular interest are cases when the BEC hosts one or multiple vortices, motivated by the possibility of impurities becoming bounded in their core or hopping across the Abrikosov lattice [21–24]. These systems naturally give rise to problems of quantum many-body physics, specifically, along the branch of polaron physics [25,26]; spectral properties of such many-body systems are ubiquitously extracted via a variety of measures broadly referred to as densities of states (DOSs)—energy distributions of excited states. We introduce and analyze a class of densities of states, which we call *hydrodynamic*, that naturally arise in this problem and which characterize the capacity of each excitation to interact with a given impurity. Moreover, we analyze the standard densities of states of Bogoliubov excitations to resolve their spectral structure (independently of the presence of an impurity). Remarkably, the latter point to the existence of anomalies in the excitation spectrum at small momenta, which are rooted in the long-range profile of the vortex.

In this paper, we provide a detailed investigation of the low-lying spectrum of excitations of a quasi-2D BEC supporting a single-charge, on-axis vortex (vortex BEC) by means of DOSs and local densities of states (LDOSs) alike. The hydrodynamic LDOS, introduced here, follows from the leading-order coupling of an impurity to the excitations of a BEC. These measures show the exceptional sensitivity of an impurity to the remnant kelvon mode [27], also known as the lowest core-localized state (LCLS) [8], and to the Nambu-Goldstone mode of the spontaneous symmetry breaking of the phase degree of freedom of a BEC. We show that the action of a pinning potential, which we include as the stabilization mechanism of the vortex [8,28], affords a degree of quantum-level control over an impurity trapped in the core of the vortex mediated by the LCLS.

The paper is organized as follows: in Sec. II A, we review the Bogoliubov formalism applied to a vortex BEC. We compute the relevant densities of states in Sec. II B, where we introduce the Bogoliubov and hydrodynamic DOS, followed by a description of the physical setup in Sec. II C. Numerical results are shown in Sec. III, where we highlight the spectral features of the vortex BEC by comparison with the homogeneous, zero-vorticity case. Conclusion and discussion follow in Sec. IV.

II. FORMULATION

A. Bogoliubov formalism for a vortex BEC

We begin by considering the field-quantized Hamiltonian

$$\hat{H} = \int d^2r\, \hat{\Phi}^\dagger(\mathbf{r})\left[-\frac{\hbar^2}{2M}\nabla^2 - \mu + V(\mathbf{r})\right]\hat{\Phi}(\mathbf{r}) + \frac{1}{2}g\int d^2r\, \hat{\Phi}^\dagger(\mathbf{r})\hat{\Phi}^\dagger(\mathbf{r})\hat{\Phi}(\mathbf{r})\hat{\Phi}(\mathbf{r}), \tag{1}$$

describing the field of a bosonic species of mass M interacting by an effective contact potential of strength $g > 0$. Atomic annihilation and creation operators $\hat{\Phi}$ and $\hat{\Phi}^\dagger$ satisfy the commutation relation $[\hat{\Phi}(\mathbf{r}), \hat{\Phi}^\dagger(\mathbf{r}')] = \delta(\mathbf{r} - \mathbf{r}')$ and $\hat{N} = \int d^2r\, \hat{\Phi}^\dagger(\mathbf{r})\hat{\Phi}(\mathbf{r})$ is the number operator, the expectation value of which is fixed by the chemical potential μ. The external potential V is composed of two contributions: a highly anisotropic trapping potential $V_{\rm tr}$, rendering the system quasi-2D, and a small pinning potential $V_{\rm p}$, introduced here to energetically stabilize the vortex. (These potentials are detailed in Sec. II C.)

The Bogoliubov approach suffices in the case of a weakly interacting BEC [29]. We thus decompose the field as

$$\begin{pmatrix}\hat{\Phi}(\mathbf{r})\\ \hat{\Phi}^\dagger(\mathbf{r})\end{pmatrix} = \sqrt{n_0}\begin{pmatrix}\Phi_0(\mathbf{r})\\ \overline{\Phi_0}(\mathbf{r})\end{pmatrix} + \begin{pmatrix}\hat{\phi}(\mathbf{r})\\ \hat{\phi}^\dagger(\mathbf{r})\end{pmatrix}, \tag{2}$$

where Φ_0 is a BEC wave function ($\overline{\Phi_0}$ its complex conjugate), on top of which $\hat{\phi}(\mathbf{r})$ ($\hat{\phi}(\mathbf{r})^\dagger$) annihilates (creates) quantum excitations. Here, $n_0 = N_0/\mathcal{A}$, with N_0 the number of BEC atoms and $\mathcal{A}$ the area covered by the quasi-2D BEC cloud. The mean-field Φ_0 satisfies the time-independent Gross-Pitaevskii (GP) equation,

$$(h - \mu + n_0 g|\Phi_0|^2)\Phi_0 = 0, \tag{3}$$

with $h = -(\hbar^2/2M)\nabla^2 + V$, subject to the boundary condition consistent with the external potential V and to the normalization condition

$$\langle\hat{N}\rangle_0 = n_0\int d^2r\, |\Phi_0(\mathbf{r})|^2 = N_0, \tag{4}$$

where $\langle\ldots\rangle_0$ represents the expected value in the many-body state of the BEC, which can be used to determine μ.

We choose the natural microscopic units to be the coupling energy $n_0 g$ and the healing length $\xi = \hbar/\sqrt{2Mn_0 g}$, so that quantities in the Hamiltonian (1) become rescaled as $\mathbf{r} \mapsto \xi\mathbf{r}$, $\hat{\Phi} \mapsto \xi^{-1}\hat{\Phi}$, $\mu \mapsto (n_0 g)\mu$, $h \mapsto (n_0 g)h$, and $\hat{H} \mapsto (n_0\xi^2)(n_0 g)\hat{H}$; substituting for (2) and by virtue of (3), we have

$$\hat{H} = F_0 + \frac{1}{n_0\xi^2}\hat{H}_{\rm B} + \ldots \tag{5}$$

where $F_0 = \int d^2r\, \overline{\Phi_0}(h - \mu + \frac{1}{2}|\Phi_0|^2)\Phi_0$ is the (classical) free energy of the BEC and

$$\hat{H}_{\rm B} = \frac{1}{2}\int d^2r \begin{pmatrix}\hat{\phi}\\ \hat{\phi}^\dagger\end{pmatrix}^\dagger \sigma_3\mathcal{H}_{\rm B}\begin{pmatrix}\hat{\phi}\\ \hat{\phi}^\dagger\end{pmatrix} \tag{6}$$

with the Bogoliubov operator

$$\mathcal{H}_{\rm B} = \sigma_3\begin{pmatrix}h - \mu + 2|\Phi_0|^2 & \Phi_0^2\\ \overline{\Phi_0}^2 & h - \mu + 2|\Phi_0|^2\end{pmatrix}, \tag{7}$$

where σ_i $(i = 1, 2, 3)$ denote Pauli matrices. Higher-order contributions of Eq. (5) are neglected within the Bogoliubov approximation. This requires $\langle\hat{N}\rangle_0 \approx \langle\hat{N}\rangle$, which holds provided $k_B T \ll \mu$ and $n_0\xi^2 \gg 1$, i.e., in the limit of both weak thermal and quantum depletions. We then expand the excitation operators as

$$\begin{pmatrix}\hat{\phi}(\mathbf{r})\\ \hat{\phi}^\dagger(\mathbf{r})\end{pmatrix} = \sum_{\lambda=0}^{\infty}[X_\lambda(\mathbf{r})\hat{b}_\lambda + \sigma_1\overline{X_\lambda}(\mathbf{r})\hat{b}_\lambda^\dagger], \tag{8}$$

in a complete basis of complex vector-valued functions $X_\lambda(\mathbf{r}) = (u_\lambda(\mathbf{r}), v_\lambda(\mathbf{r}))^T$ ($\overline{X_\lambda}$ its complex conjugate), the components u_λ and v_λ of which are the particle and hole components, respectively. By requiring that each $\hat{b}_\lambda$ and $\hat{b}_\lambda^\dagger$ inherits bosonic commutation relations, the diagonalization of (6) becomes an eigenproblem for the X_λ as

$$\mathcal{H}_{\rm B}X_\lambda = \omega_\lambda X_\lambda. \tag{9}$$

Bogoliubov operators $\mathcal{H}_{\rm B}$ are non-Hermitian and, in general, admit complex eigenvalues [2]; the operator we study presently, however, possesses a fully real spectrum [5] and the biorthonormality relations

$$\langle X_\lambda, X_{\lambda'}\rangle = \int d^2r\, X_\lambda^\dagger\sigma_3 X_{\lambda'} = \delta_{\lambda,\lambda'}, \tag{10}$$

$$\langle\sigma_1\overline{X_\lambda}, X_{\lambda'}\rangle = \int d^2r\, (\sigma_1\overline{X_\lambda})^\dagger\sigma_3 X_{\lambda'} = 0 \tag{11}$$

hold for every normalized eigenstate, where we introduce the bilinear product $\langle\cdot,\cdot\rangle$; the diagonalized form of (6) thus reads

$$\hat{H}_{\rm B} = \frac{1}{2}\alpha\hat{P}^2 + \sum_{\lambda\neq 0}\omega_\lambda\hat{b}_\lambda^\dagger\hat{b}_\lambda, \tag{12}$$

where the first term accounts for the dynamics of the phase degree of freedom of the BEC [12]. We explain the structure and importance of this term by observing that the variation of Eq. (4), i.e.,

$$\delta\langle\hat{N}\rangle_0 = \delta N_0, \tag{13}$$

yields the condition

$$\int\frac{d^2r}{\mathcal{A}}\,(\overline{\Phi_0}\Theta_0 + \Phi_0\overline{\Theta_0}) = 1, \tag{14}$$

where we introduce the adjoint BEC wave function

$$\Theta_0(\mathbf{r}) = \left(N_0\frac{\partial\mu}{\partial N_0}\right)\frac{d\Phi_0}{d\mu}(\mathbf{r}). \tag{15}$$

It is because Eq. (3) holds that Φ_0 and Θ_0 comprise, respectively, the zero mode of $\mathcal{H}_{\rm B}$ (the Nambu-Goldstone mode of the BEC state [30]) and its adjoint, as

$$\mathcal{H}_{\rm B}\begin{pmatrix}\Phi_0\\ -\overline{\Phi_0}\end{pmatrix} = 0, \quad \mathcal{H}_{\rm B}\begin{pmatrix}\Theta_0\\ \overline{\Theta_0}\end{pmatrix} = \alpha\begin{pmatrix}\Phi_0\\ -\overline{\Phi_0}\end{pmatrix}. \tag{16}$$

The second of these equations is obtained by taking the derivative $d/d\mu$ of the first and then multiplying it by α, where we identify $\alpha \equiv N_0(\partial\mu/\partial N_0)$ [12]. These solutions make up the $\lambda = 0$ mode in (8) as $X_0 = (\Theta_0 + \Phi_0, \overline{\Theta_0} - \overline{\Phi_0})^T/\sqrt{2\mathcal{A}}$, which is normalized, per Eq. (14), as $\langle X_0, X_0\rangle = 1$, thus determining α. The associated operators $\hat{b}_0$ and $\hat{b}_0^\dagger$ comprise the Hermitian operator $\hat{P} = \frac{1}{\sqrt{2}}(\hat{b}_0 + \hat{b}_0^\dagger)$ [31]. Notice that, by

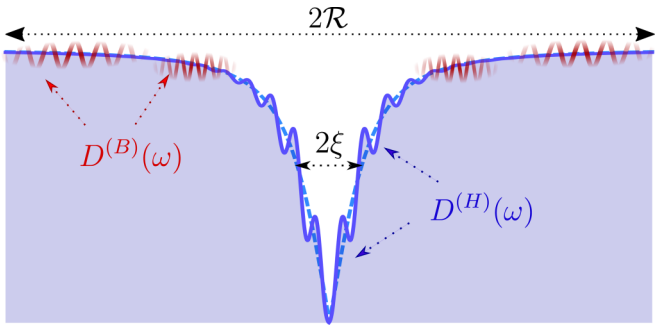

FIG. 1. Schematic representation of the excitations on top of a quantum vortex (blue solid line and red wiggly lines). The quasi-2D BEC has a width $2\mathcal{R}$ and hosts a vortex of width 2ξ the mean-field solution of which, computed in the absence of excitations or impurities, is depicted for comparison (blue dashed line). The Bogoliubov and the hydrodynamic densities of states $D^{(\mathrm{B})}$ and $D^{(\mathrm{H})}$ (see Sec. II B) are based on two distinct pictures of excitations: $D^{(\mathrm{B})}(\omega)$ characterizes an excitation of frequency ω as a matter wave excited from the BEC background, or vacuum (red wiggly lines), while $D^{(\mathrm{H})}(\omega)$ characterizes the same excitation but as a rippling of the BEC density (solid blue line). As such, the latter is directly affected by the presence of the vortex.

following from Eq. (13), the adjoint wave function's defining physical condition, Eq. (14), informs us of its role in the variations (or, fluctuations) of the number of BEC atoms. Number fluctuations are a necessary consequence of the definite phase acquired by the BEC upon breaking the gauge symmetry of the Hamiltonian (1), as phase and particle number are conjugate degrees of freedom. Hence the meaning of the $\hat{P}^2$ term in Eq. (12) is explained: it encapsulates the zero-energy dynamics of the BEC's phase. For conciseness, we refer to the mode X_0 as the NG mode henceforth. The basis (8) thus becomes complete. (The zero mode pertaining to the position of the vortex core, though related to the present discussion, is present only when the vortex is off axis [32].)

Making the potential V be isotropic in the plane and assuming a vortex to be on the axis of a disk-shaped quasi-2D BEC, a vortex solution of the GP Eq. (3) can be written in polar coordinates as

$$\Phi_\nu(r,\varphi) = e^{i\nu\varphi}\phi_\nu(r), \tag{17}$$

where ν is an integer, the quantized vorticity, and ϕ_ν satisfies a reduced form of Eq. (3) in the radial coordinate [33]. The form of $|\phi_\nu(r)|^2$ is sketched in Fig. 1 and plotted in Fig. 2 below. Inserting (17) in Eq. (7), it becomes apparent that solutions of Eq. (9) can be separated, in polar coordinates, as

$$X_\lambda(r,\varphi) = e^{i\varphi(m+\nu\sigma_3)}X_{m,n}(r), \tag{18}$$

where m is an integer, the angular momentum of the excitation, and n, the number of nodes in the radial coordinate, is the quantum number associated to the nonzero eigenstates of the reduced Bogoliubov operator

$$\sigma_3\mathcal{H}_m = \begin{pmatrix} h-\mu+2\phi_\nu^2 & \phi_\nu^2 \\ \phi_\nu^2 & h-\mu+2\phi_\nu^2 \end{pmatrix} + \frac{1}{r^2}(m+\nu\sigma_3)^2, \tag{19}$$

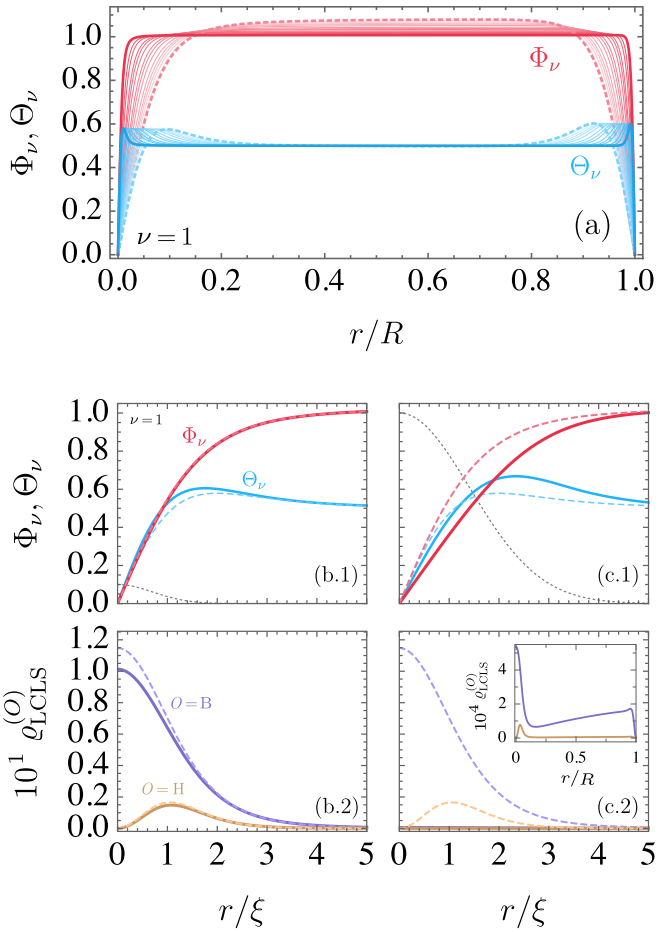

FIG. 2. Panel (a) shows plots of the wave functions of the BEC Φ_ν (red) and of its adjoint Θ_ν (blue) for $\nu = 1$ in absence of a pinning potential, for system sizes ranging between $R = 20$ (dashed) and $R = 200$ (solid), across the entire radial dimension of the system. The region near the vortex core is shown in subpanels (b.1) and (b.2) for a configuration of the pinning potential $(\epsilon, w) = (0.1, 1)$ and in subpanels (c.1) and (c.2) for $(\epsilon, w) = (1, 2)$. (b.1), (c.1) Wave functions of the BEC Φ_ν (red) and of its adjoint Θ_ν (blue), where black dotted lines plot the profile of the pinning potential V_{p} for each of the configurations. (b.2), (c.2) Spatial densities of the LCLS $\varrho^{(O)}_{\mathrm{LCLS}}$ from the Bogoliubov (solid purple, $O = \mathrm{B}$) and the hydrodynamic (solid orange, $O = \mathrm{H}$) LDOS; the inset in subpanel (c.2) shows the spatial densities at a smaller scale across the entire radial dimension, since they become invisible at the scale of the plot and delocalized from the vortex core (as explained in Appendix A); for comparison, dashed lines plot the respective spatial densities in absence of a pinning potential.

acting on $X_{m,n}(r) = (\alpha_{m,n}(\mathbf{r}), \beta_{m,n}(\mathbf{r}))^T$. The label $\lambda \neq 0$ is, thus, explicitly identified with the pair of quantum numbers (m, n) of solutions of the eigenproblem

$$\mathcal{H}_m X_{m,n} = \omega_{m,n} X_{m,n}. \tag{20}$$

Note that, by Eqs. (15) and (16), the NG mode has angular momentum $m = 0$.

B. Densities of states

The LDOS of Bogoliubov excitations is typically defined in terms of the imaginary part of the associated Green's function [34]. In particular, we can consider an angular momentum-resolved LDOS (AM-LDOS), given by

$$D_m^{(\mathrm{B})}(\mathbf{r};\omega) = \sum_n \varrho_{m,n}^{(\mathrm{B})}(\mathbf{r})\delta(\omega-\omega_{m,n}), \tag{21}$$

with the spatial density $\varrho_{m,n}^{(\mathrm{B})}$ given by

$$\varrho_{m,n}^{(\mathrm{B})}(\mathbf{r}) = |u_{m,n}(\mathbf{r})|^2 - |v_{m,n}(\mathbf{r})|^2. \tag{22}$$

However, a test particle of a different species (i.e., an atomic impurity) that interacts with the species comprising the BEC can be found to be sensitive to an AM-LDOS of a distinct form:

$$D_m^{(\mathrm{H})}(\mathbf{r};\omega) = \sum_n \varrho_{m,n}^{(\mathrm{H})}(\mathbf{r})\delta(\omega-\omega_{m,n}), \tag{23}$$

with the spatial density $\varrho_{m,n}^{(\mathrm{H})}$ given by

$$\varrho_{m,n}^{(\mathrm{H})}(\mathbf{r}) = |\overline{\Phi}_0(\mathbf{r})u_{m,n}(\mathbf{r}) + \Phi_0(\mathbf{r})v_{m,n}(\mathbf{r})|^2, \tag{24}$$

which is due, physically, to the interactions with the bosonic system being exclusively density interactions. The derivation of this AM-LDOS is illustrated in Appendix B. We shall refer to the quantities in, and derived from, Eqs. (21) and (23) as the Bogoliubov and the hydrodynamic densities of states, respectively. We coin the latter *hydrodynamic* densities due to the $\varrho_{m,n}^{(\mathrm{H})}$ being identical to the density degree of freedom used in the hydrodynamic formalism for the excitations of a BEC [35].

Associated to the LDOS is the DOS, which provides a measure for counting excitations of a many-body system [29]. The angular momentum-resolved DOS (AM-DOS) is obtained by integrating in space each of the AM-LDOS, yielding

$$D_m^{(O)}(\omega) = \sum_n c_{m,n}^{(O)}\delta(\omega-\omega_{m,n}), \tag{25}$$

where $O = \mathrm{B}, \mathrm{H}$, with weights $c_{m,n}^{(\mathrm{B})} = 1$ for the Bogoliubov densities of states, by virtue of Eq. (10), and

$$c_{m,n}^{(\mathrm{H})} = \int d^2r\, \varrho_{m,n}^{(\mathrm{H})}(\mathbf{r}) \tag{26}$$

for the hydrodynamic density of states. The (total) LDOS and DOS are recovered upon summing over all m, i.e.,

$$D^{(O)}(\omega) = \sum_m D_m^{(O)}(\omega) \tag{27}$$

for the DOS; as in Eq. (25), this is for $O = \mathrm{B}, \mathrm{H}$. Figure 1 shows a sketch of the two distinct pictures, or interpretations, of the Bogoliubov excitations as characterized by the Bogoliubov and the hydrodynamic DOS.

For comparison with numerical results, we consider a large, homogeneous (i.e., vorticity zero and no boundary effects) quasi-2D BEC, in which case excitations have the Bogoliubov dispersion $\omega_B(\mathbf{k}) = \sqrt{k^2(2\mu+k^2)}$, with $\mathbf{k}$ the mode's wave vector, or momentum, and $k = \|\mathbf{k}\|$. The Bogoliubov and the hydrodynamic DOS of excitations of the homogeneous quasi-2D BEC can then be explicitly computed in the continuum approximation of momentum space, i.e., approximating the sum over modes by an integral over $\mathbf{k}$, yielding

$$D_{\mathrm{hom}}^{(\mathrm{B})}(\omega) = \frac{A}{4\pi}\frac{\omega}{\sqrt{\mu^2+\omega^2}} = \frac{A}{4\pi}\frac{\omega}{\mu} - O(\omega^3), \tag{28}$$

$$D_{\mathrm{hom}}^{(\mathrm{H})}(\omega) = \frac{\mu A}{4\pi}\left(1-\frac{\mu}{\sqrt{\mu^2+\omega^2}}\right) = \frac{A}{8\pi}\frac{\omega^2}{\mu} - O(\omega^4), \tag{29}$$

with $A = \mathcal{A}/\xi^2$ the area covered by the BEC in natural units.

C. Vortex nucleation and external potentials

We envision the on-axis vortex to be nucleated by phase imprinting via Laguerre-Gauss beams [36], that is, without imposing any laboratory-frame rotation on the fluid.

We consider the anisotropy of the trapping potential V_{tr} to be produced by a tight harmonic potential in the z direction of energy $\hbar\omega_z \gg k_{\mathrm{B}}T$, yielding the effective interaction strength $g = \sqrt{8\pi}\hbar^2 a/(M l_z)$, where $a > 0$ is the s-wave scattering length and $l_z = \sqrt{\hbar/(M\omega_z)}$ is the characteristic length of the harmonic potential.

The in-plane radial trap is a box potential of radius $\mathcal{R} \gg \xi$, making Eq. (3) subject to the boundary condition $\Phi_0(\mathcal{R},\varphi) = 0$. We motivate the choice of a box potential by virtue of its capacity to render an essentially homogeneous BEC [37,38]: because we are interested in *intrinsic* properties of the vortex and its quantum excitations in the plane, we seek to avoid any possible extrinsic effects caused by a harmonic potential. Then, in the natural units, the radius $\mathcal{R} = R\xi$ is given by $R = \sqrt{N/(\pi n_0\xi^2)}$, where $n_0\xi^2 = l_z/(4\sqrt{2\pi}a)$ is independent of the in-plane radial size (R is related to a dimensionless coupling strength introduced in Refs. [4,39]). For the pinning potential, we consider $V_{\mathrm{p}}(r) = \epsilon\exp(-r^2/w^2)$, i.e., a Gaussian beam with maximum optical potential ϵ and waist length w [8,40]; we shall refer to pinning configurations in terms of the ordered pair (ϵ, w).

For the numerical calculations, we consider experiments with ^{7}Li BECs [41] wherein positive values of a of tens of nanometers are accessible via Feshbach resonances. For instance, at $a = 10$ nm and $\omega_z = 100$ kHz we have $l_z \approx 300$ nm and $n_0\xi^2 = 3$; the Bogoliubov approximation is valid, but there may be residual quantum depletion effects in the realization of this particular BEC. Then, in these settings, a BEC of $N = 2\times10^5$ atoms yields $R \approx 150$, while experiments with box potentials up to $\mathcal{R} = 35$ μm [42] yield, in laboratory units, $n_0 g/\hbar \approx 78$ kHz, or $n_0 g/k_{\mathrm{B}} \approx 600$ nK, and $\xi \approx 240$ nm.

III. RESULTS

We give an account of our numerical analysis of the quantities presented in Sec. II B. We begin by briefly explaining the numerical methods used and the motivation for the inclusion of a pinning potential. Then, we present and discuss results for the Bogoliubov and the hydrodynamic DOS, Eq. (27) for $O = \mathrm{B}, \mathrm{H}$, where we will encounter details that motivate an investigation of the low-lying states of definite angular momentum. Using the AM-DOS and the AM-LDOS, we make the physical origin of the hydrodynamic signatures clear.

Finally, we provide a scaling analysis through which we identify anomalies in the low-lying excitation spectrum.

A. Numerical vortex solutions

Combining Eqs. (3) and (17) yields the reduced radial equation

$$\left(h+\frac{\nu^2}{r^2}-\mu+\phi_\nu^2(r)\right)\phi_\nu(r)=0. \tag{30}$$

We generate numerical solutions of (30) for $\nu=1$ using a combination of imaginary-time evolution and an R-asymptotic approximation, as outlined in Appendix C; results are presented in Fig. 2(a). We then use these to obtain numerical solutions of Eq. (20) using a discretization-based solver.

Single-charge (i.e., $|\nu|=1$) vortices are *dynamically stable*, meaning that the associated Bogoliubov operator (7) possesses only real eigenvalues. However, due to a negative energy of the LCLS, they are *energetically unstable*, meaning that the spectrum of $\hat{H}_{\rm B}$, Eq. (12), has a negative eigenvalue and, therefore, that the mean-field (30) is energetically unstable. The existence of the LCLS has long been recognized and known to trigger the vortex's spiraling-out motion [3–11]. In Fig. 2 we show features of the BEC wave function and its adjoint near the vortex core, as well as the Bogoliubov and hydrodynamic spatial densities of the LCLS.

B. Total densities of states

Figure 3 shows plots of the Bogoliubov and the hydrodynamic DOS for multiple values of R and fixed (ϵ, w). We have chosen to represent the Dirac delta function in Eqs. (21) by a Lorentz distribution,

$$\delta(\omega)\sim\frac{1}{\pi}\frac{\delta\omega}{\omega^2+\delta\omega^2},$$

with the width $\delta\omega=O(R^{-2})$; this width is of the energy scale of a single particle in a rigid wall potential of size R and yields the Dirac delta in the limit $R\to\infty$. We see that, apart from noise, the numerical results are in good agreement with the analytical results in Eqs. (28) and (29) for the homogenous BEC.

Both $D^{(\rm B)}_{\rm hom}$ and $D^{(\rm H)}_{\rm hom}$ deviate from the numerical result only in the low-energy region of the spectrum, around $\omega\approx 0$, as shown in the insets of Fig. 3. This deviation is twofold.

(i) The low-lying hydrodynamic DOS is dominated by a peak at energy $\omega_{-1,0}$ of the LCLS (or remnant kelvon mode) [inset of Fig. 3(b)].

(ii) The Bogoliubov DOS shows that the energy $\omega_{0,0}=\omega_{0,0}(R)$, the energy of the first *nonkelvonic* excitation, appears to become larger than the typical interlevel spacing with increasing R [highlighted in the inset of Fig. 3(a)].

Additionally, the presence of the NG mode (especially notable in the hydrodynamic DOS) is not inconsistent with the Bogoliubov spectrum $\omega_B(\mathbf{k})$, which accounts only for density excitations. (Although excitations of the Bogoliubov spectrum entail phase excitations, the NG mode is an excitation of the phase *exclusively*.)

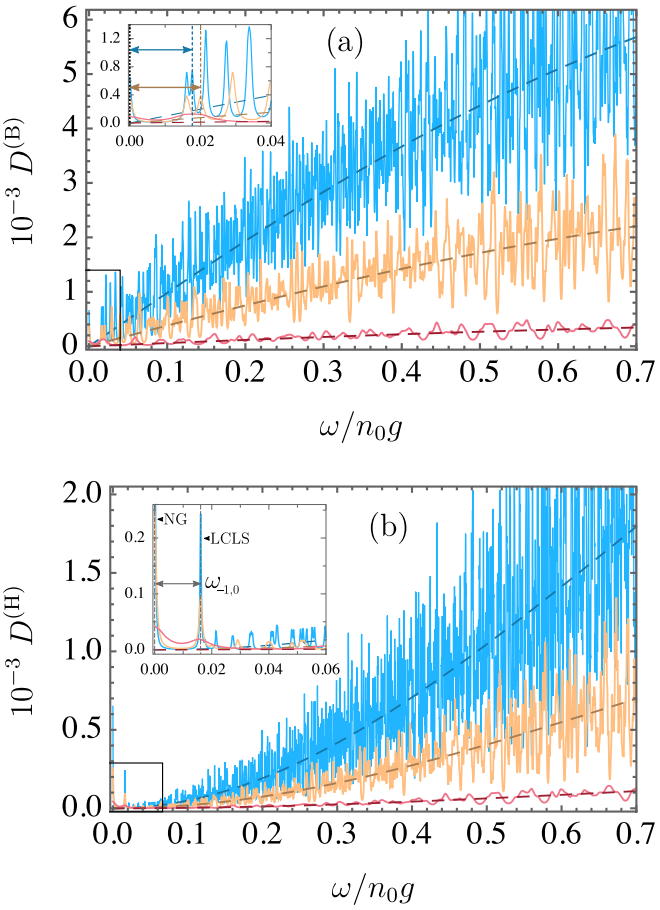

FIG. 3. Plots of the (a) Bogoliubov and (b) hydrodynamic DOS (solid), compared with the plots of Eqs. (28) and (29) (dashed), for system sizes $R=50$ (red), $R=125$ (orange), and $R=200$ (blue) (appearing in ascending order in the plots), and pinning $(\epsilon, w)=(0.1, 1)$. Distinct scales in the vertical axes show that $D^{(\rm B)}$ bounds $D^{(\rm H)}$. Insets zoom into the low-energy features in the boxed regions of the respective plots: (a) the highlighted energies are the energy of the first density (nonkelvonic) excitation $\omega_{0,0}$ for the two system sizes $R=125$ and 200 and (b) peaks belonging to the NG mode and LCLS are labeled; the energy $\omega_{-1,0}$ is the energy of the LCLS at the selected configuration of the pinning potential. The notation of the energy levels follows Eq. (20).

C. Angular momentum-resolved densities of states

1. AM-DOS

Figure 4 shows plots of the AM-DOS for selected values of (ϵ, w) and R and angular momenta $m=0,\pm1,\pm2$. Notable features of the hydrodynamic DOS are reproduced here: the NG mode, at $m=0$, and the LCLS, at $m=-1$, tower over all other low-lying states.

There is a visible growth of the hydrodynamic weight, Eq. (26) (the height of the peaks in each $D^{(\rm H)}_m$), with energy that ties in with the known breakdown of the hydrodynamic approximation beyond low energies [29]: it signals a departure from a collective sound-wave (phononic) picture of excitations, wherein the spectrum is $\sim k$, to a single-particle (atomic) one, with the spectrum $\sim k^2$. The transition from the phononic to the atomic picture is accompanied by a decrease in the

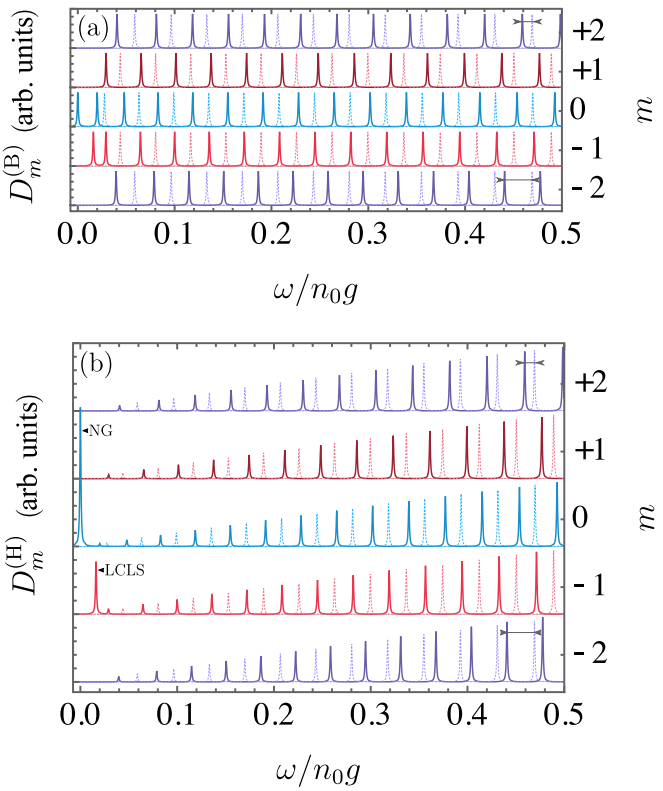

FIG. 4. Plots of the (a) Bogoliubov and (b) hydrodynamic AM-DOS for angular momenta $m = 0, \pm 1, \pm 2$ at system size $R = 125$ and pinning $(\epsilon, w) = (0.1, 1)$. Dotted lines are the corresponding AM-DOS for the fully homogeneous BEC in Eqs. (28) and (29). (b) Peak intensities are proportional to the hydrodynamic weights $c_{m,n}^{(H)}$; within the energy range plotted, the largest is $c_{NG}^{(H)} \approx 0.5$ of the Nambu-Goldstone mode. In the plots for $m = \pm 2$ we have marked energy differences with respect to the homogeneous BEC to highlight the lifting of angular momentum degeneracy by the vortex.

magnitude of the hole component v_λ relative to the particle component u_λ of the excitation [29]. Thus, in this sense, the hydrodynamic weight $c^{(H)}$, Eq. (26), is a measure of the particle-hole imbalance of a bosonic state. We explain this observation by noting that the hydrodynamic spatial density $\varrho_\lambda^{(H)}$, Eq. (24), amounts to an *interference pattern* between the amplitudes of the particle and hole components u_λ and v_λ; this interference is essentially destructive, since $\Phi_0 v_\lambda$ has only a phase $e^{i\pi}$ relative to $\overline{\Phi}_0 u_\lambda$. Thus, the discrepancy between the magnitudes of u_λ and v_λ determines the intensity of the interference pattern $\varrho_\lambda^{(H)}$ and then $c_\lambda^{(H)}$, being its integral, functions as a *global* measure of the particle-hole *imbalance* of the mode X_λ.

We note, moreover, that the presence of the vortex is known to lift the angular momentum-degenerate excitations of an otherwise homogeneous BEC [35], a feature that we highlight in Fig. 4.

2. AM-LDOS

In contrast to the DOS, the AM-DOSs of a finite system are sparse (compare Figs. 3 and 4), that is, states are separable within each angular momentum sector. It follows that the spatial dimension of the AM-LDOS can be represented faithfully in terms of individual spatial densities $\varrho_{m,n}^{(O)}$, Eqs. (22) and (24), alone. These are displayed in Fig. 5. In particular, the Bogoliubov density of the LCLS is shown to be orders of magnitude larger at the core than other low-lying, core-localized states.

This happens because $\varrho^{(B)}$ in Eq. (22) is sign indefinite, so that a bosonic state can be locally particlelike (holelike) in regions of positive (negative) sign; accordingly, the state is locally characterized by an accumulation (depletion) of atoms proportional to its magnitude. Complementarily to the hydrodynamic weight $c^{(H)}$, which acts as a global measure, the Bogoliubov spatial density $\varrho^{(B)}$ acts as a *local* measure of particle-hole *character* of a state. The LCLS is, therefore, largely more particlelike ($|u_{LCLS}| \gg |v_{LCLS}|$) than most other low-lying states [4], whence its hydrodynamic weight derives exceptional magnitude. The one exception is the NG mode, which is likewise particlelike but delocalized: its Bogoliubov AM-LDOS is similar in magnitude to that of the first nonkelvonic excitation, for instance, but the hydrodynamic

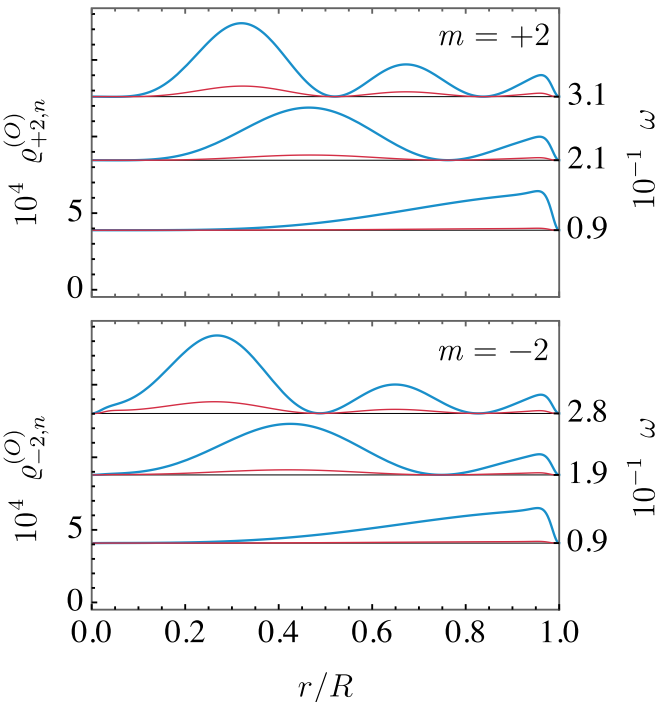

FIG. 5. Plots of the Bogoliubov (blue, $O = B$) and hydrodynamic (red, $O = H$) spatial densities for the first few states of angular momentum $m = 0, \pm 1, \pm 2$ at system size $R = 50$ and pinning $(\epsilon, w) = (0.1, 1)$, representing the AM-LDOS at each value $\omega = \omega_{m,n}$ along the right-vertical axes. Magnitudes of spatial densities can be inferred from the scale on the left-vertical axis of each panel; each Bogoliubov spatial density has locally a larger magnitude than its hydrodynamic counterpart. $m = \pm 2$: Densities are nearly identical except at $r \approx 0$ (more visible with increasing energies). $m = +1$: The Bogoliubov density is holelike (negative) at $r \approx 0$. $m = 0$: The lowest state (NG mode) is plotted in distinct colors—purple for $O = B$, orange for $O = H$; unlike most other states, the hydrodynamic spatial density is comparable with its Bogoliubov counterpart. $m = -1$: The lowest state (LCLS) is plotted in likewise distinct colors and in dotted lines, shown here for comparison—a clearer picture is displayed in Fig. 2(b.2); here, the Bogoliubov density is purposefully shown to exceed the plot range.

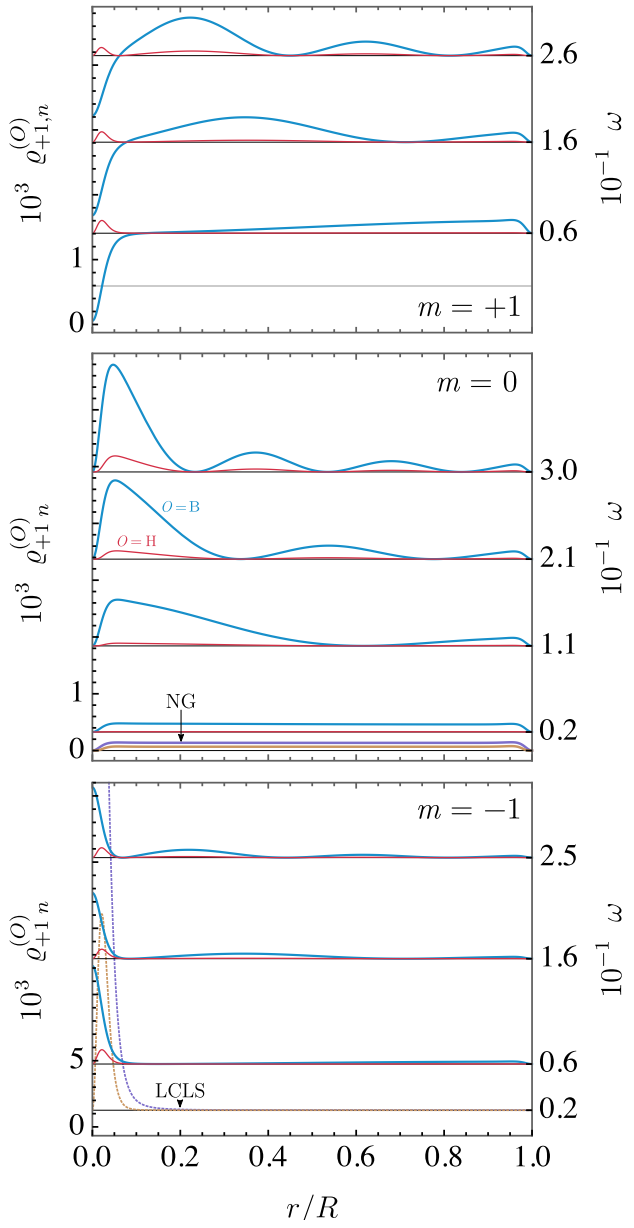

FIG. 5. *(Continued.)*.

AM-DOS of the latter is vanishing—in fact, the hydrodynamic weight of the first is negligible while that of the NG surpasses the LCLS (see Fig. 4). As energy increases, the magnitudes of the Bogoliubov and hydrodynamic densities become generically comparable, as modes become progressively more particlelike. These features are patent in Fig. 5.

We carried out a detailed study of the dependence of the LCLS on the pinning potential parameters (ϵ, w), shown in Appendix A. In particular, we explicate the outsized effect of this external potential on the LCLS in relation to the negligible effect on every other mode of the system. Moreover, we show that the pronounced LCLS peak shown in Fig. 4 becomes diluted as we push it into the energy range of the nonkelvonic density excitations, which is a consequence of increasing the intensity of the pinning potential.

D. Scaling and R dependence

We carried out scaling analyses concerning the discrepancy between the gap (that is, the energy of the lowest nonkelvonic excitation $\omega_{0,0}$) and the mean interlevel spacing $\Delta\omega$, as apparent in the inset of Fig. 3(a). Thus, we obtained information on the appropriate low-energy, continuum description of density excitations; results are shown in Fig. 6. Indeed, we find distinct scalings between the energy of the first density excitation and the mean interlevel spacing, indicative of a gap that scales anomalously as $O(R^{-1/2})$. For comparison, we show the prediction for a homogeneous BEC (given by the Bogoliubov spectrum ω_B) to scale as R^{-1}; this gap is a trivial finite-size effect, as it scales equally to the mean interlevel spacing and approaches a massless spectrum. Notice that the deviation in the exponent of the mean interlevel spacing from that of the homogeneous spectrum, though small, is not accounted for by the error margin. Considering that the group velocity must vanish at the gap, this deviation is suggestive of a nonanalytic, momentum-dependent correction to the linear dispersion.

Finally, it is shown in Fig. 8 of Appendix A that the energy level of the LCLS does not cross zero at the presented system size, that is, that it does not represent an energetic instability. Indeed, we have found that this mode stabilizes spontaneously for a system size $R \gtrsim 73$, in qualitative agreement with Ref. [4]. (Eventual quantitative discrepancies are attributed to the fact that a quasi-2D BEC produced by a box potential is considered here.)

IV. DISCUSSION AND CONCLUSIONS

We have acquired insights into the spectral properties of a quantum vortex in a quasi-2D BEC by analyzing the Bogoliubov and hydrodynamic densities of states. Our discussion was particularly focused on two modes of the system: on the one hand, the lowest core-localized state, which is the remnant kelvon mode surviving the dimensionality reduction imposed by the trap; and, on the other hand, the Nambu-Goldstone mode inherent to the BEC state. Most strikingly, we have shown that these modes have an exceptional capacity to interact with impurities embedded in the BEC. Therefore, they can have a sizable influence on the dynamics of these impurities or, more generally, heterogeneous atomic species. Regarding the NG mode, we propose that this effect may be observable in the dynamics of degenerate fermion-BEC mixtures as well as heterogeneous BEC mixtures [43–46]. A proper account of the NG mode also becomes important to the polaron physics of the impurity-BEC system, as impurities can become exceptionally sensitive to the phase fluctuations of the BEC. Physically, this effect is rooted in the particular way excitations interact with an impurity, the strength of which results from an interference pattern between their particle and hole components.

The LCLS will greatly affect impurities trapped in the core of the vortex due to its localized character. It can stimulate transitions between quantum states of the impurity, be they orbital states or internal degrees of freedom, by virtue of the LCLS being an eigenstate of angular momentum. In turn, the LCLS is highly sensitive to the action of a pinning potential (see Appendix A; this is the physical fundament of that

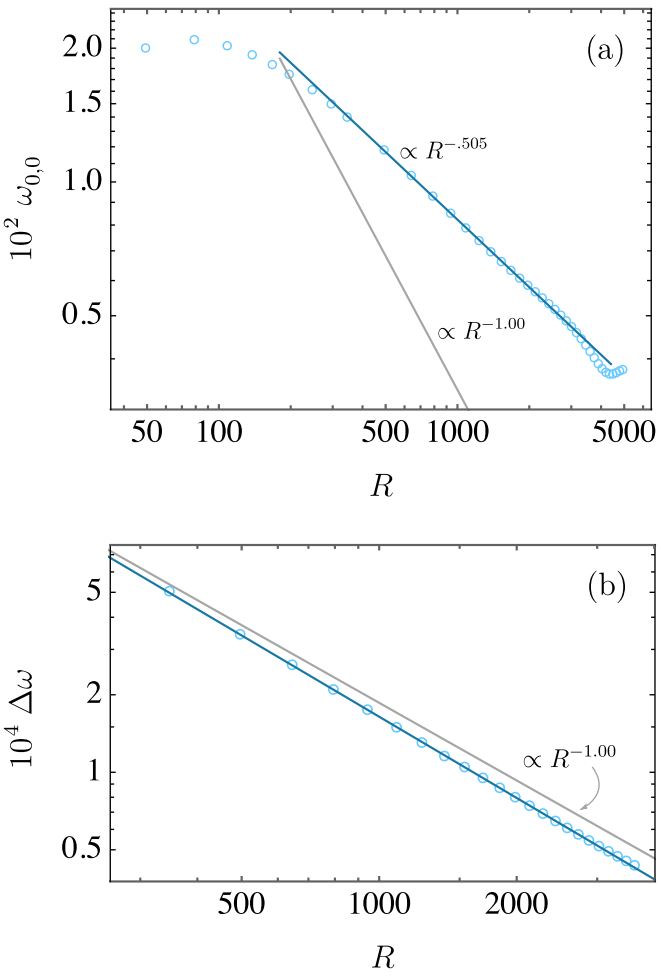

FIG. 6. Log-log plots of (a) $\omega_{0,0}$, the energy of the first nonkelvonic excitation without a pinning potential, and (b) $\Delta\omega$, the mean interlevel energy spacing between states above $\omega_{0,0}$, as functions of R; light blue circles are the numerical data and the darker blue lines are the linear fits performed in the scaling region used to obtain the exponents $\alpha = -0.505 \pm 0.002$ for $\omega_{0,0}^{(0)}$ and $\beta = -1.05 \pm 0.03$ for $\Delta\omega$; the latter we obtained from a fixed sample including the first 250 states above $\omega_{0,0}$ and, in the fitting, we considered the standard error of the mean. Data break away from the scaling region at very large R plausibly due to numerical errors, as local features become too small to be resolved at the defined numerical precision. Gray lines in each panel are the corresponding quantity obtained from the homogeneous system used to derive Eqs. (28) and (29), the energy levels of which are given explicitly in terms of the homogeneous spectrum by $\omega_{m,n} = \omega_B(k_{m,n})$ and $k_{m,n} = j_{m,n+1}/R$ where $j_{m,n+1}$ is the $(n+1)$th zero of the Bessel function J_m; deviations from the R^{-1} scaling are one order of magnitude below significant digits and covered by error margins. Finally, we point out that the scaling exponent $\beta \approx -1.05$ is not to be taken at face value but, rather, that it reflects a logarithmic correction [1].

mechanism of vortex stabilization [8,28]). It follows that the LCLS affords a mechanism of control over a vortex-trapped impurity at the quantum level: its energy can be tuned to a transition between two states of distinct angular momentum of the impurity, by means of the pinning potential, and can stimulate the transition. As a matter of fact, there is no fundamental reason for this mechanism to be limited to the single-vortex configuration considered presently—we can expect local properties of the excitations to hold in different physical setups. For instance, in the Abrikosov lattice of a quasi-2D BEC, each vortex in the array is bound to possess a qualitatively similar remnant kelvon mode [47] and the array is amenable to pinning and manipulation by an optical lattice [48,49]. By allowing for such a degree of local, quantum-level control, this channel may be of practical use for a proposal based on vortex-trapped impurities as qubit units for quantum information processing [22,50,51].

Based on the Bogoliubov DOS and by means of a scaling analysis, we have inferred anomalies in the spectrum of excitations, namely, that the excitations of a large (but finite) BEC hosting a vortex are slightly (but nonvanishingly) gapped. This is anomalous with respect to the typical Bogoliubov spectrum, which is gapless and linear. One implication of a gapped dispersion is that the group velocity must vanish at the gap. Our scaling analysis of the mean interlevel spacing is consistent with this condition: it presents a non-negligible deviation from linearity, suggesting a nonanalytic dependence in momentum. Physically, we attribute these results to the nonlocal, long-range profile of the vortex: its decay at $\approx 1/r^2$ results in the $\log(R)$-divergent energy of the BEC and, notably, in a logarithmically modified dispersion of its kelvons (in a three-dimensional BEC) [1]. To our knowledge, however, the theory to support the long-wavelength dispersion of the in-plane, nonkelvonic density excitations is yet to be established. This may be important to the quantum treatment of vortex dynamics in a quasi-2D BEC [52] and in optical lattices, wherein a gap pertaining to motion of the vortex has been reported [53].

ACKNOWLEDGMENTS

The authors acknowledge the financial support of Fundação para a Ciência e Tecnologia through Grant No. PD/BD/128625/2017, Contract No. CEECIND/00401/2018, Grant No. UID/CTM/04540/2019, Project No. PTDC/FIS-OUT/3882/2020, and Grant No. COVID/BD/151814/2021. H.T. further acknowledges financial support from the Quantum Flagship Grant PhoQuS (Grant No. 820392) of the European Union. J.E.H.B. is grateful to Ana Valdés and Francisco Salces for resourceful input on experimental setups.

APPENDIX A: EFFECT OF THE PINNING POTENTIAL

The following results show how the LCLS is strongly dependent on the pinning potential, while other modes have only a negligible (and indirect) dependence. We begin by noting that the pinning energy competes against the dominant centrifugal barrier $(m + \nu\sigma_3)^2/r^2$ at the vortex core $r \lesssim 1$ in Eq. (19). A mode (m, n) is, thus, insensitive to the pinning as long as it cannot penetrate the centrifugal barrier: there may be a non-negligible dependence on the pinning potential only in case $\omega_{m,n} \gtrsim (m \pm \nu)^2$. This observation ensures that we will find a negligible effect for all low-energy modes except at angular momenta $m = \pm 1$; we have found the numerical evidence to support this observation, and so we focus our

discussion on the case $m = -1$, for definiteness. In Fig. 6, we depict the eigenvalues and hydrodynamic weights $c^{(\mathrm{H})}$, Eq. (26) (shown as the size of plot markers), at low energies, as functions of the pinning parameters. The strong dependence of the LCLS on the pinning potential is visible and, furthermore, we see that the $c^{(\mathrm{H})}$ cross over at avoided level crossings, suggesting that the LCLS enters the energy region of (nonkelvonic) density excitations. In order to clarify these features, we derived the minimal model described next.

We consider the reduced Bogoliubov Eq. (20) with the Hamiltonian rewritten as $\mathcal{H} = \mathcal{H}^{(0)} + \Delta\mathcal{H}$, where

$$\Delta\mathcal{H} = \sigma_3 V_{\mathrm{p}} + \sigma_3 \delta_{\mathrm{BEC}}, \tag{A1}$$

with

$$\delta_{\mathrm{BEC}} = \begin{pmatrix} -\delta\mu + 2\delta\phi^2 & \delta\phi^2 \\ \delta\phi^2 & -\delta\mu + 2\delta\phi^2 \end{pmatrix} \tag{A2}$$

(we omit subscripts $m = -1$ and $\nu = 1$ within this section), where $\delta\mu = \mu - \mu_0$ and $\delta\phi^2 = \phi^2 - \phi_0^2$; in the absence of a pinning potential, ϕ_0 and μ_0 are solutions of the GP Eq. (3) and $\mathcal{H}^{(0)}$ is the reduced Hamiltonian. Therefore, the term δ_{BEC} is understood as a potential energy due to the *deformation* of the BEC caused by the applied pinning potential.

The first level avoidance involves the $m = -1$ modes $X_n^{(0)}$, for $n = 0, 1$ solutions of $\mathcal{H}^{(0)} X_n^{(0)} = \omega_n^{(0)} X_n^{(0)}$. Thus, we expand the eigenstates of (20) in this subspace, i.e,

$$X(r) = a_0 X_0^{(0)}(r) + a_1 X_1^{(0)}(r). \tag{A3}$$

Taking the bilinear product $\langle X_i^{(0)}, \mathcal{H}X\rangle$, for $i = 0, 1$, yields the algebraic equation

$$\begin{pmatrix} \omega_0^{(0)} + \Delta_{00} & \Delta_{01} \\ \Delta_{10} & \omega_1^{(0)} + \Delta_{11} \end{pmatrix} \begin{pmatrix} a_0 \\ a_1 \end{pmatrix} = \omega \begin{pmatrix} a_0 \\ a_1 \end{pmatrix},$$

where $\Delta_{ij} = \Delta_{ji} = \langle X_i^{(0)}, \Delta\mathcal{H} X_j^{(0)}\rangle$, with the eigenvalues

$$\omega_{n=0,1} = \tilde{\omega} + \Delta_+ \mp \sqrt{(\Omega - \Delta_-)^2 + |\Delta_{01}|^2}, \tag{A4}$$

where $\tilde{\omega} = (\omega_1^{(0)} + \omega_0^{(0)})/2$, the half gap $\Omega = (\omega_1^{(0)} - \omega_0^{(0)})/2$, and $\Delta_\pm = (\Delta_{00} \pm \Delta_{11})/2$; the minus-signed (plus-signed) branch in Eq. (A4) is the $n = 0$ ($n = 1$) solution. The comparisons of Eqs. (A4) with the numerical results in Fig. 7 reveal the qualitative agreement of the minimal model; the quantitative inaccuracy results simply from the truncated subspace in Eq. (A3) and is of no bearing to the following analysis.

Further comparing Eq. (A4) with numerics in Fig. 7, we observe Δ_{00} to be much larger than Δ_{01} and Δ_{11}; indeed, we found $\Delta_{01} \approx 10^{-2}\Delta_{00}$ while $10^{-2} < \Delta_{11}/\Delta_{01} \lesssim 1$ across the sampled values of (ϵ, w). To clarify these disparities, we consider the quantity

$$\eta_{ij} = \frac{\langle X_i^{(0)}, \sigma_3 \delta_{\mathrm{BEC}} X_j^{(0)}\rangle}{\langle X_i^{(0)}, \sigma_3 V_{\mathrm{p}} X_j^{(0)}\rangle},$$

that is, the ratio of the contributions to the Δ_{ij}, Eq. (A1): the term V_{p} is the potential energy due to the pinning potential; the term δ_{BEC}, Eq. (A2), is the potential energy due to the deformation of the BEC caused by the pinning potential. (Note that both terms are effects of the application of the pinning potential on the system, but that V_{p} is the *direct* effect

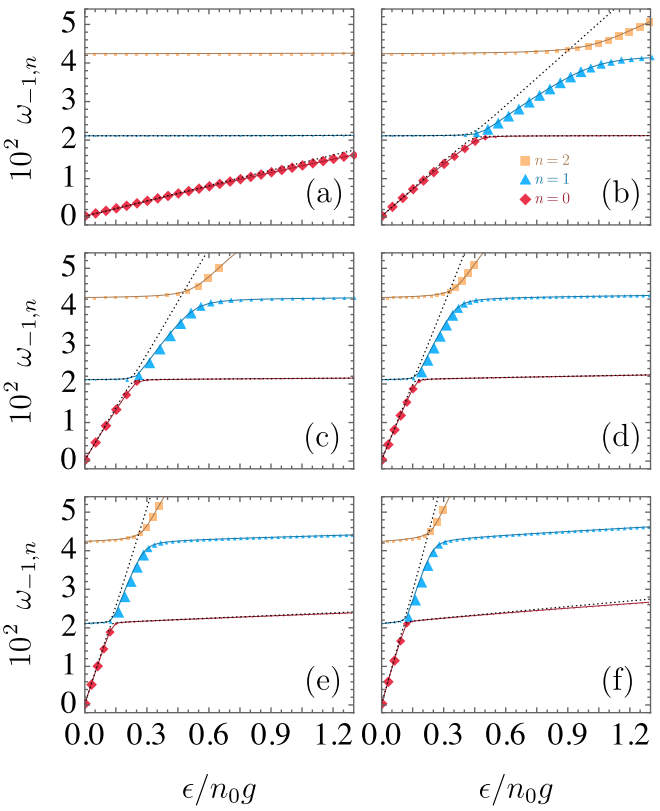

FIG. 7. Plots of eigenvalues $\omega_{m,n}$ of the modes $n = 0, 1, 2$ of angular momentum $m = -1$ as a function of the maximum optical potential ϵ, for $R = 200$ and beam waist (a) $w = 0.2$, (b) $w = 0.4$, (c) $w = 0.6$, (d) $w = 0.8$, (e) $w = 1.0$, and (f) $w = 1.2$; the size of the plot markers is proportional to the hydrodynamic weight, Eq. (26), of each state, for each value of ϵ (scaled logarithmically for comparison). Black dotted lines show the results of the minimal model described in the text.

while δ_{BEC} is an *indirect* effect on its modes, in particular.) We found that $\eta_{11} > 0$ with $0.1 < \eta_{11} < 20$ and, for $i = 0, 1$, $\eta_{0i} < 0$ (negative due to the deformation term) with $10^{-2} < |\eta_{0i}| < 0.5$, increasing with w in all cases—that is, the term V_{p} dominates over δ_{BEC} for both Δ_{00} and Δ_{01} and vice versa for Δ_{11}. This shows, since $\Delta_{00} \gg \Delta_{01} \gg \Delta_{11}$, that the LCLS is strongly dependent on the pinning potential *directly*, due to its exceptionally large amplitude at the vortex core; other modes are, at most, negligibly dependent on the pinning potential and *indirectly* so via the deformation of the BEC, as shown by Δ_{11}.

We analyze the crossover of the $c^{(\mathrm{H})}$ by considering the probability of observing the pinning potential-free LCLS (i.e., the state $X_0^{(0)}$) given a state X_n, that is, the overlap $|a_{0,n}|^2 = |\langle X_0^{(0)}, X_n\rangle|^2$, plotted in Fig. 8. This figure of merit differentiates the states that possess a large, particlelike density at the vortex core for each configuration of the pinning potential. In particular, we can conclude that the LCLS (i.e., the mode with quantum numbers $m = -1$ and $n = 0$) eventually loses the characteristic hydrodynamic weight resulting from the large, core-localized density, as this becomes, due to the pinning potential, a feature of higher-energy states. Hence we see the negligible magnitude of the $\varrho_{\mathrm{LCLS}}^{(O)}$ seen in Fig. 2(c.2) relative to Fig. 2(b.2). Moreover, we notice that the crossover $a_{0,0}$

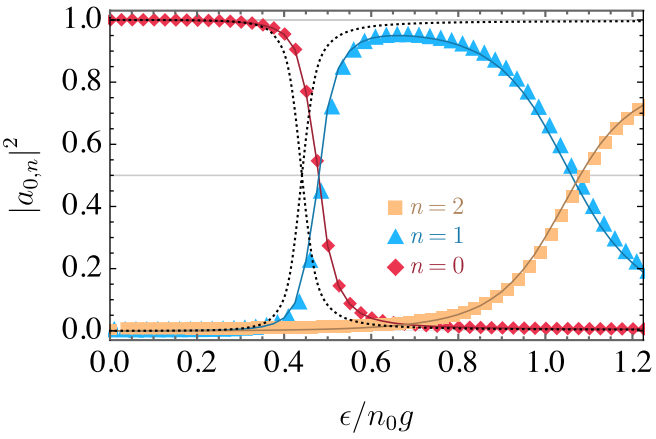

FIG. 8. Plots of overlaps $|a_{0,n}|^2 = |\langle X_0^{(0)}, X_n\rangle|^2$ of modes $n = 0, 1, 2$ of angular momentum $m = -1$ with the $n = 0$ mode of the pinningless system, as a function of the maximum optical potential ϵ for system size $R = 200$ and beam waist $w = 0.4$ [same as Fig. 7(b)]. Black dotted lines show the results of the minimal model described in the text. The curve for $n = 3$ is not included, though it is visible that $a_{0,3}$ becomes non-negligible within this range.

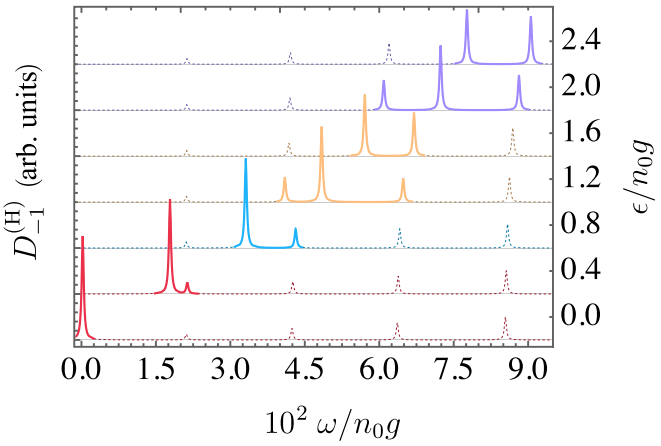

FIG. 9. Hydrodynamic AM-DOS of low-energy modes of angular momentum $m = -1$ as a function of the maximum optical potential ϵ (right-vertical axis) for system size $R = 200$ and beam waist $w = 0.4$ [same as Fig. 7(b)]. Solid lines highlight modes that have a noticeably increased hydrodynamic weight $c^{(\mathrm{H})}$, for each value of ϵ, and colors indicate the mode having the largest hydrodynamic weight with red ($n = 0$), blue ($n = 1$), orange ($n = 2$), and violet ($n = 3$). The fact that the energy of the LCLS is positive in the absence of a pinning potential ($\epsilon = 0$) is addressed in Sec. III D.

with $a_{0,1}$ is relatively steep while $a_{0,1}$ with $a_{0,2}$ is markedly smoother and can be seen to take place at a value $|a_{0,2}|^2 < 0.5$. This suggests that, as the intensity of the pinning potential increases (and with it the energy of a density at the vortex core), the large hydrodynamic weight characteristic of the LCLS (for a weak pinning potential) becomes spread out across a number of modes instead of concentrated in a single one, and, so, there will be a number of modes with increased hydrodynamic weights instead of a single dominant one. Thus, we can think of the large hydrodynamic weight, initially concentrated in the LCLS, as becoming diluted under a sufficiently intense pinning potential. This effect is shown in terms of the hydrodynamic AM-DOS in Fig. 9.

APPENDIX B: DECAY WIDTH OF AN IMPURITY BOUNDED IN A QUANTUM VORTEX

We motivate the introduction of the hydrodynamic densities of states, Eqs. (23), (25), and (27), by obtaining the decay width between bound states of an impurity in a quantum vortex.

We consider the BEC described by Hamiltonian (1) to be in the presence of atoms of a distinct species, described by a Hamiltonian

$$\hat{H}_{\mathrm{imp}} = \int d^2 r\, \hat{\Psi}^\dagger(\mathbf{r})\left[-\frac{\hbar^2}{2M_2}\nabla^2 + g_{12}\hat{\Phi}^\dagger(\mathbf{r})\hat{\Phi}(\mathbf{r})\right]\hat{\Psi}(\mathbf{r}), \tag{B1}$$

that is, a field of dilute (i.e., noninteracting) atoms of mass M_2 interacting with BEC atoms by a contact potential of strength $g_{12} > 0$; we identify the atoms of mass M_2 as impurities with respect to the BEC, since they are assumed to be dilute and of a distinct species; the total Hamiltonian will be $\hat{H} = \hat{H}_{\mathrm{BEC}} + \hat{H}_{\mathrm{imp}}$.

Substituting the BEC fields for (2) in (B1) yields, to leading and subleading orders,

$$\hat{H}_{\mathrm{imp}} = \frac{\chi}{n_0\xi^2}\int d^2 r\, \hat{\Psi}^\dagger h_{\mathrm{imp}}\hat{\Psi} + \frac{\chi\gamma^2}{(n_0\xi^2)^{\frac{3}{2}}}\int d^2 r\, \hat{\Psi}^\dagger(\overline{\Phi}_\nu\hat{\phi} + \Phi_\nu\hat{\phi}^\dagger)\hat{\Psi} + \ldots, \tag{B2}$$

scaled to the natural units $n_0 g$ and ξ, according to the prescriptions in the main text, having introduced a Schrödinger operator $h_{\mathrm{imp}} = -\nabla^2 + \gamma^2|\Phi_\nu|^2$ and parameters $\chi = M/M_2$ and $\gamma^2 = M_2 g_{12}/(Mg)$; performing a further scaling $\hat{H}_{\mathrm{imp}} \mapsto \frac{\chi}{n_0\xi^2}\hat{H}_{\mathrm{imp}}$, the total Hamiltonian can be written as

$$\hat{H} = F_0 + \frac{1}{n_0\xi^2}(\hat{H}_{\mathrm{B}} + \chi\hat{H}_{\mathrm{imp}}).$$

Bosonic field operators $\hat{\phi}$ and $\hat{\phi}^\dagger$ are expanded as in Eq. (8), a basis of eigenfunctions of $\mathcal{H}_{\mathrm{B}}$, resulting in

$$\overline{\Phi}_\nu(\mathbf{r})\hat{\phi}(\mathbf{r}) + \mathrm{H.c.} = \sum_{m,n}(\zeta_{m,n}(\mathbf{r})\hat{b}_{m,n} + \overline{\zeta_{m,n}}(\mathbf{r})\hat{b}^\dagger_{m,n}),$$

$$\zeta_{m,n}(\mathbf{r}) = \overline{\Phi}_\nu(\mathbf{r})u_{m,n}(\mathbf{r}) + \Phi_\nu(\mathbf{r})v_{m,n}(\mathbf{r}),$$

where the identification $\lambda = (m, n)$ is made. Impurity field operators $\hat{\Psi}$ and $\hat{\Psi}^\dagger$ can be expanded in a basis of eigenfunctions of h_{imp}: the vortex profile of the BEC density $|\Phi_\nu|^2$—along with the condition that $g_{12} > 0$—essentially guarantees the existence of bound states of the impurities localized at the vortex core [22]; these are also eigenstates of angular momentum in the plane, since the density $|\Phi_\nu|^2$ is cylindrically symmetric

For the purpose of this derivation, we consider a two-level truncated basis composed of the lowest-energy states

of angular momenta $\ell \neq 0$ and $\ell' = 0$, i.e., we let $\hat{\Psi}(\mathbf{r}) = \Psi_0(\mathbf{r})\hat{a}_0 + \Psi_\ell(\mathbf{r})\hat{a}_\ell$, yielding the effective Hamiltonian

$$\hat{H}_{\text{eff}} = \hat{H}_{\text{B}} + \Delta(\hat{a}_\ell^\dagger \hat{a}_\ell - \hat{a}_0^\dagger \hat{a}_0) + \sum_{m,n} \left(g_{\ell,0}^{(n)} \hat{b}_{m,n} + g_{0,\ell}^{(n)} \hat{b}_{m,n}^\dagger\right) \hat{a}_\ell^\dagger \hat{a}_0 + \text{H.c.}, \tag{B3}$$

with 2Δ the energy gap, where $g_{\ell,0}^{(n)} = \delta_{\ell,m} g_\ell^{(n)}$ and $g_{0,\ell}^{(n)} = \delta_{-\ell,m} g_{-\ell}^{(n)}$, with

$$g_\ell^{(n)} = \frac{\chi\gamma^2}{\sqrt{n_0\xi^2}} \int d^2r\, \overline{\Psi}_\ell \zeta_{\ell,n} \Psi_0\,;$$

the selection rules above are made apparent from the fact that $L\zeta_{m,n} = m\zeta_{m,n}$ and $L\Psi_\ell = \ell\Psi_\ell$, with $L = -i\partial/\partial\varphi$ the two-dimensional angular momentum operator. An effective model for the dynamics of the impurity coupled to the bosonic bath follows from (B3) by projecting onto a single-particle subspace of the impurity in the rotating-wave approximation and considering only the bosonic modes of angular momentum $m = \ell$:

$$\hat{H}_{\text{eff}} = \sum_n \omega_{\ell,n} \hat{b}_{\ell,n}^\dagger \hat{b}_{\ell,n} + \Delta\sigma_3 + \sum_n \left(e^{-it(\omega_{\ell,n}-\Delta)} g_\ell^{(n)} \hat{b}_{\ell,n}\sigma_+ + \text{H.c.}\right),$$

with σ_+ the raising operator of impurity levels. A standard approach to this problem is to employ the Wigner-Weisskopf approximation [54], which predicts a decay width

$$\Gamma_{\ell\to 0} = \pi \sum_n \left|g_\ell^{(n)}\right|^2 \delta(\Delta - \omega_{\ell,n}).$$

Then, considering that the impurity is localized in the vortex core of a large BEC, the $|g_\ell^{(n)}|^2$ can be approximated to rewrite the width as

$$\Gamma_{\ell\to 0} \approx \pi \frac{\chi^2\gamma^4}{n_0\xi^2} \int d^2r\, D_\ell^{(\text{H})}(\mathbf{r};\Delta) |\Psi_\ell(\mathbf{r})|^2 |\Psi_0(\mathbf{r})|^2,$$

where $D_\ell^{(\text{H})}(\mathbf{r};\Delta) = \sum_n |\zeta_{\ell,n}(\mathbf{r})|^2 \delta(\Delta - \omega_{\ell,n})$ is a hydrodynamic AM-LDOS, Eq. (23).

APPENDIX C: COMPUTATION OF THE RADIAL BEC PROFILE

A box potential, such as considered in this paper, endows the BEC wave function with a nearly homogeneous profile, with the exception of an exponentially fast depletion of the wave function at the border [55]. On the one hand, as the size of the BEC increases, it becomes numerically nontrivial to compute its full profile, seeing as the depletion becomes steeper and more abrupt at the scale of the system, as illustrated in Fig. 2(a); on the other hand, provided that any other nonhomogeneous feature is sufficiently localized within the bulk, that is, away from the border of the BEC, the computation of its wave function in the bulk and the computation of the wave function near the border can be asymptotically separated. We employ this observation to compute the solution of Eq. (30) by introducing an ansatz of the form

$$\phi_\nu(r) = \phi_\Sigma(r)\phi_{\partial\Sigma}(r),$$

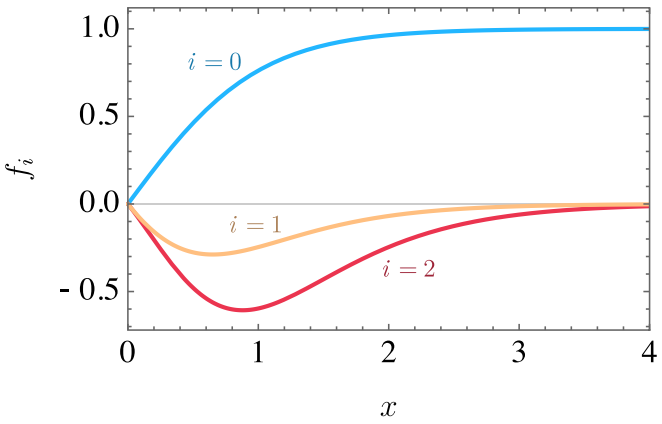

FIG. 10. Asymptotic solutions f_i, for orders $i = 0, 1, 2$, of Eq. (C1) for $\nu = 1$ and $\mu \gtrsim 1$.

where ϕ_Σ is the wave function in the bulk surface of the quasi-2D BEC and $\phi_{\partial\Sigma}$ is the wave function near the border.

The bulk wave function ϕ_Σ is required to satisfy Eq. (30) in absence of V_{tr}—that is, it is not required to satisfy the boundary condition $\phi_\nu(R) = 0$, but rather $\phi_\Sigma(r \to \infty) = \sqrt{\mu}$ by the asymptotic separation argument. The solution can be obtained using imaginary-time evolution on a transformed radial coordinate $\theta = 2\arctan(r)$, with $\theta \in [0, \pi)$; we did not update the chemical potential at each step of the evolution [56] but rather sampled the parametric μ dependence of the numerical solutions. Further, because V_{p} is exponentially localized at the origin, the asymptotic expansion $\phi_\Sigma(r) = \sqrt{\mu}(1 - \frac{\nu^2}{2\mu r^2}) + \ldots$ holds for large r [33].

We now solve for $\phi_{\partial\Sigma}$ using an asymptotic approximation. We begin by writing $\phi_{\partial\Sigma}(r) = f(x)$, for $i = 0, 1, 2$, with the coordinate $x = \sqrt{\mu/2}(R - r)$; the resulting equation reads

$$-\frac{1}{2}f'' + \left(\frac{1}{\sqrt{2\mu}}\frac{1}{R} + \frac{x}{\mu R^2}\right)f' + \frac{\nu^2}{\mu R^2}f - \left[1 - \left(1 - \frac{\nu^2}{\mu R^2}\right)f^2\right]f = O(R^{-3}), \tag{C1}$$

where we keep terms up to second order in R^{-1}; likewise, we expand f asymptotically to order R^{-2}:

$$f(x) = f_0(x) + R^{-1}f_1(x) + R^{-2}f_2(x) + \ldots. \tag{C2}$$

Considering $x \in [0, \infty)$ by the asymptotic separation argument, we require the boundary condition $f(0) = 0$ and that $f(x)$ be bounded as $x \to \infty$. To zeroth order, the equation is $-\frac{1}{2}f_0'' - (1 - f_0^2)f_0 = 0$, with solution $f_0(x) = \tanh(x)$, in agreement with Ref. [55]. The first- and second-order equations are not worth displaying here; we mention only that we solved for the f_i analytically with the aid of symbolic computation software; results are plotted in Fig. 10.

This method was validated against fully imaginary time-evolved solutions for small system sizes ($R < 70$). Because R^2 amounts to a dimensionless coupling strength [4], this approximation constitutes a strong-coupling approximation.

[1] L. P. Pitaevskii, Zh. Eksp. Teor. Fiz. **40**, 646 (1961) [Sov. Phys. JETP **13**, 451 (1961)].
[2] Y. Kawaguchi and T. Ohmi, Phys. Rev. A **70**, 043610 (2004).
[3] F. Dalfovo and S. Stringari, Phys. Rev. A **53**, 2477 (1996).
[4] D. S. Rokhsar, Phys. Rev. Lett. **79**, 2164 (1997).
[5] T. Isoshima and K. Machida, J. Phys. Soc. Jpn. **66**, 3502 (1997).
[6] R. J. Dodd, K. Burnett, M. Edwards, and C. W. Clark, Phys. Rev. A **56**, 587 (1997).
[7] A. L. Fetter, J. Low Temp. Phys. **113**, 189 (1998).
[8] T. Isoshima and K. Machida, Phys. Rev. A **59**, 2203 (1999).
[9] P. O. Fedichev and G. V. Shlyapnikov, Phys. Rev. A **60**, R1779 (1999).
[10] A. A. Svidzinsky and A. L. Fetter, Phys. Rev. Lett. **84**, 5919 (2000).
[11] S. M. M. Virtanen, T. P. Simula, and M. M. Salomaa, Phys. Rev. Lett. **86**, 2704 (2001).
[12] M. Lewenstein and L. You, Phys. Rev. Lett. **77**, 3489 (1996).
[13] J. Tempere, W. Casteels, M. K. Oberthaler, S. Knoop, E. Timmermans, and J. T. Devreese, Phys. Rev. B **80**, 184504 (2009).
[14] N. B. Jørgensen, L. Wacker, K. T. Skalmstang, M. M. Parish, J. Levinsen, R. S. Christensen, G. M. Bruun, and J. J. Arlt, Phys. Rev. Lett. **117**, 055302 (2016).
[15] S. M. Yoshida, S. Endo, J. Levinsen, and M. M. Parish, Phys. Rev. X **8**, 011024 (2018).
[16] M. Drescher, M. Salmhofer, and T. Enss, Phys. Rev. A **99**, 023601 (2019).
[17] S. I. Mistakidis, G. C. Katsimiga, G. M. Koutentakis, T. Busch, and P. Schmelcher, Phys. Rev. Lett. **122**, 183001 (2019).
[18] L. A. Peña Ardila, N. B. Jørgensen, T. Pohl, S. Giorgini, G. M. Bruun, and J. J. Arlt, Phys. Rev. A **99**, 063607 (2019).
[19] O. Hryhorchak, G. Panochko, and V. Pastukhov, J. Phys. B **53**, 205302 (2020).
[20] M. M. Khan, H. Terças, J. T. Mendonça, J. Wehr, C. Charalambous, M. Lewenstein, and M. A. Garcia-March, Phys. Rev. A **103**, 023303 (2021).
[21] T. H. Johnson, Y. Yuan, W. Bao, S. R. Clark, C. Foot, and D. Jaksch, Phys. Rev. Lett. **116**, 240402 (2016).
[22] J. E. H. Braz and H. Terças, Phys. Rev. A **101**, 023607 (2020).
[23] M. Edmonds, M. Eto, and M. Nitta, Phys. Rev. Res. **3**, 023085 (2021).
[24] A. Richaud, V. Penna, R. Mayol, and M. Guilleumas, Phys. Rev. A **101**, 013630 (2020).
[25] A. Alexandrov and J. Devreese, *Advances in Polaron Physics* (Springer-Verlag, Berlin, 2010).
[26] D. Emin, *Polarons* (Cambridge University, Cambridge, England, 2012).
[27] T. Simula, Phys. Rev. A **97**, 023609 (2018).
[28] T. Isoshima and K. Machida, J. Phys. Soc. Jpn. **68**, 487 (1999).
[29] F. Dalfovo, S. Giorgini, L. P. Pitaevskii, and S. Stringari, Rev. Mod. Phys. **71**, 463 (1999).
[30] H. Matsumoto and S. Sakamoto, Prog. Theor. Phys. **107**, 679 (2002).
[31] J.-P. Blaizot and G. Ripka, *Quantum Theory of Finite Systems* (MIT, Cambridge, MA, 1986), Vol. 3.
[32] T. M. Wright, A. S. Bradley, and R. J. Ballagh, Phys. Rev. A **80**, 053624 (2009).
[33] N. Manton and P. Sutcliffe, *Topological Solitons* (Cambridge University Press, Cambridge, 2004).
[34] G. Mahan, *Many-Particle Physics* (Springer, New York, 2013).
[35] A. A. Svidzinsky and A. L. Fetter, Phys. Rev. A **58**, 3168 (1998).
[36] M. F. Andersen, C. Ryu, P. Cladé, V. Natarajan, A. Vaziri, K. Helmerson, and W. D. Phillips, Phys. Rev. Lett. **97**, 170406 (2006).
[37] A. L. Gaunt, T. F. Schmidutz, I. Gotlibovych, R. P. Smith, and Z. Hadzibabic, Phys. Rev. Lett. **110**, 200406 (2013).
[38] L. Chomaz, L. Corman, T. Bienaimé, R. Desbuquois, C. Weitenberg, S. Nascimbène, J. Beugnon, and J. Dalibard, Nat. Commun. **6**, 6162 (2015).
[39] D. A. Butts and D. S. Rokhsar, Nature (London) **397**, 327 (1999).
[40] C. Ryu, M. F. Andersen, P. Cladé, V. Natarajan, K. Helmerson, and W. D. Phillips, Phys. Rev. Lett. **99**, 260401 (2007).
[41] N. Gross and L. Khaykovich, Phys. Rev. A **77**, 023604 (2008).
[42] I. Gotlibovych, T. F. Schmidutz, A. L. Gaunt, N. Navon, R. P. Smith, and Z. Hadzibabic, Phys. Rev. A **89**, 061604(R) (2014).
[43] A. M. Belemuk, N. M. Chtchelkatchev, V. N. Ryzhov, and S.-T. Chui, Phys. Rev. A **73**, 053608 (2006).
[44] M. Eto, K. Kasamatsu, M. Nitta, H. Takeuchi, and M. Tsubota, Phys. Rev. A **83**, 063603 (2011).
[45] J. O. Indekeu, N. Van Thu, C.-Y. Lin, and T. H. Phat, Phys. Rev. A **97**, 043605 (2018).
[46] T. Mithun, K. Kasamatsu, B. Dey, and P. G. Kevrekidis, Phys. Rev. A **103**, 023301 (2021).
[47] F. Chevy and S. Stringari, Phys. Rev. A **68**, 053601 (2003).
[48] J. W. Reijnders and R. A. Duine, Phys. Rev. Lett. **93**, 060401 (2004).
[49] S. Tung, V. Schweikhard, and E. A. Cornell, Phys. Rev. Lett. **97**, 240402 (2006).
[50] M. I. Shaukat, E. V. Castro, and H. Terças, Phys. Rev. A **95**, 053618 (2017).
[51] M. I. Shaukat, E. V. Castro, and H. Terças, Phys. Rev. A **99**, 042326 (2019).
[52] T. Simula, Phys. Rev. A **101**, 063616 (2020).
[53] P. Vignolo, R. Fazio, and M. P. Tosi, Phys. Rev. A **76**, 023616 (2007).
[54] Y. K. Wang and I. C. Khoo, Opt. Commun. **11**, 323 (1974).
[55] C. J. Pethick and H. Smith, *Bose-Einstein Condensation in Dilute Gases*, 2nd ed. (Cambridge University, New York, 2008).
[56] W. Bao and Q. Du, SIAM J. Sci. Comput. **25**, 1674 (2004).